Electronic supplementary information

Mixed-dimensional light-emitting diode based on a *p*-MoS_2 nanosheet and an *n*-CdSe nanowire

S1. Investigation of the electron mobility (μ_e) and concentration (n) of CdSe NW.

The electron mobility (μ_e) can be estimated from the channel transconductance (g_m) of the CdSe NW FET, which is expressed as: $\mu_e = g_m\left[\frac{L^2}{(C_G V_{ds})}\right]$, and $g_m = \frac{\partial I_{ds}}{\partial V_g}$, where L is the channel length, C_G is the gate capacitance. The C_G can be expressed as: $C_G = \varepsilon\varepsilon_0 L \cdot \frac{W}{h}$, where ε and h is the dielectric constant and thickness of SiO_2, W is the channel width, respectively. The g_m is 95 nA/V at V_{ds} = 0.5 V (Fig. 2b in the manuscript), C_G is 5.01×10^{-17} F/m at L =3.232 μm, W =128 nm, h =285 nm (Fig. S1). Thus an electron mobility (μ_e) of μ_e = 396 $cm^2/V \cdot s$ is obtained. Electron concentration (n) can be estimated from the expression: $\sigma = ne\mu_e$. According to the I_{ds} vs V_{ds} curves (Fig. 2a in manuscript), σ = 6.28×10^3 $\Omega^{-1} \cdot m^{-1}$ with a NW diameter of 128 nm, obtaining $n = 1.00\times10^{18}$ cm^{-3}.

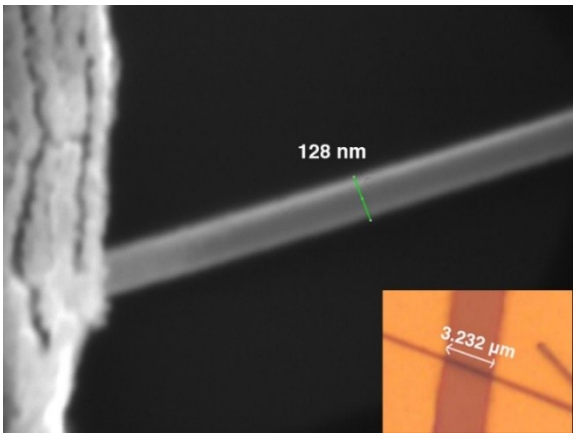

Figure S1. SEM image of the CdSe NW FET, indicating the NW diameter of 128 nm. Inset: the optical microscopy image of the single CdSe NW FET device, with a channel length of 3.232 μm.

S2. Investigation of the hole mobility (μ_h) and concentration (p) of MoS_2 NS

The hole mobility (μ_h) can be estimated from the channel transconductance (g_m) of the MoS_2 NS FET, which is expressed as: $\mu_h = g_m\left[\frac{L^2}{(C_G V_{ds})}\right]$, and $g_m = \frac{\partial I_{ds}}{\partial V_g}$, where L is the channel length, C_G is the gate capacitance. The C_G can be expressed as: $C_G = \varepsilon\varepsilon_0 L \cdot \frac{W}{h}$, where ε and h is the dielectric constant and thickness of SiO_2, W is the channel width respectively. The g_m is 52 nA/V at V_{ds} = 0.5 V (Fig 2b. in manuscript), C_G is 1.69×10^{-15} F/m at L =1.39 μm, W =10 μm, h =285 nm (Fig. S2). Thus a hole mobility (μ_h) of μ_h = 1.2 $cm^2/V \cdot s$ is obtained. Hole concentration (p) can be estimated from the expression: $\sigma = pe\mu_h$. According to the I_{ds} vs V_{ds} curves (Fig. 2a in the manuscript), σ = 311 $\Omega^{-1} \cdot m^{-1}$ with the MoS_2 NS thickness of 11 nm, obtaining p = 1.62×10^{19} cm^{-3}.

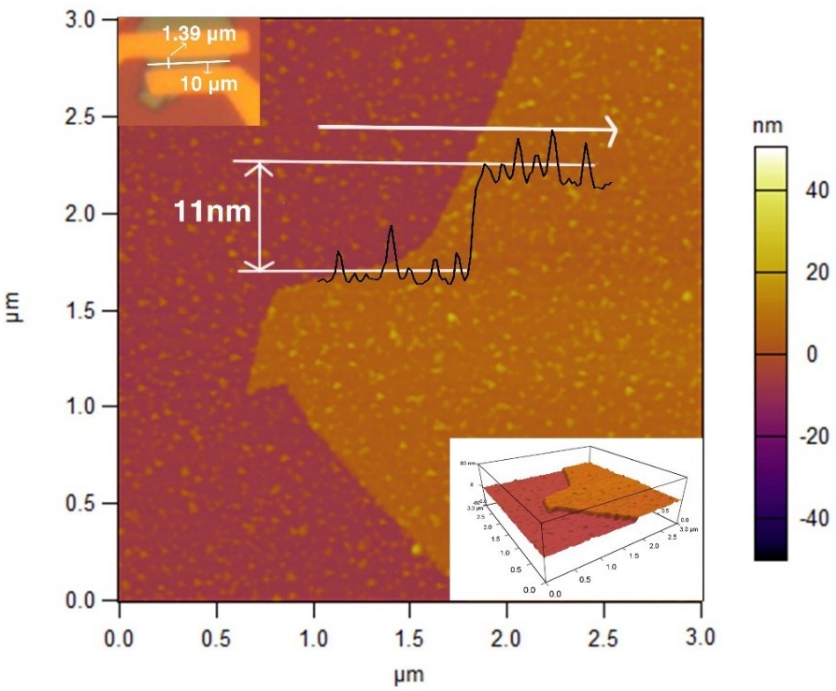

Figure S2. AFM image of MoS_2 NS, indicating a thickness of 11 nm. Inset: the optical microscopy image of the MoS_2 NS FET device with a channel length of 10 μm and channel width of 1.39 μm.

S3. Dry transfer method

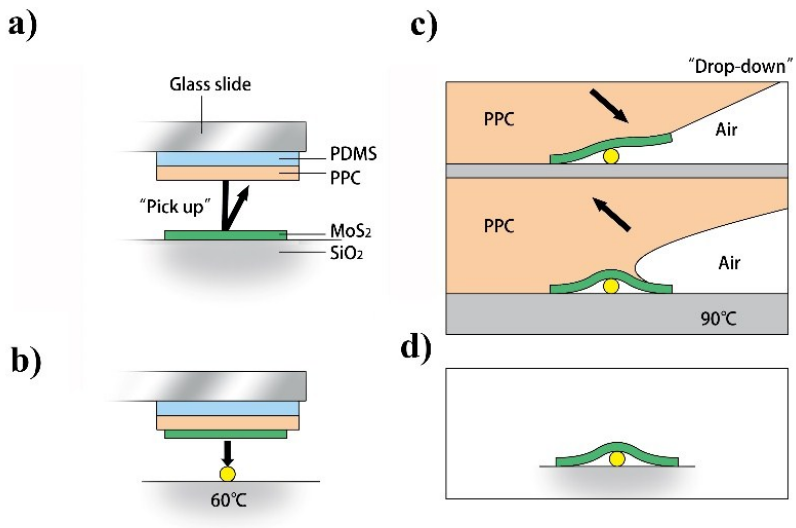

Figure S3. The schematic diagram for the dry transfer method. (a) Picking the MoS_2 nanosheet from Si/SiO_2 substrate by PPC. (b) Putting the PPC with MoS_2 nanosheet facing down onto the CdSe nanowire. (c) After the MoS_2 nanowire contacting with the CdSe nanowire, PPC was lifted off slowly. (d) Finally, the MoS_2 nanosheet will be left on the CdSe nanowire, and the 2D/1D heterostructure was formed.

As shown in Fig. S3 and Fig. S4: First, we picked up a previously exfoliated MoS_2 nanosheet from SiO_2/Si substrate by a poly dimethylsiloxane (PDMS) stamp covered by a layer of polypropylene carbonate (PPC) with the help of a glass slide at room temperature (Fig. S3a). Then, we annealed the glass slide with the stamp and MoS_2 nanosheet on top (Fig. S4c) at 90 ℃ for 1min. After that, we put the PPC with MoS_2 facing down onto the target CdSe nanowire slowly at 60 ℃ (Fig. S3b and Fig. S4d). When the MoS_2 nanosheet covered the CdSe nanowire, the SiO_2/Si substrate was heated up to 90 ℃ and the PPC was slowly lifted off (Fig. S3c and Fig. S4e). Finally, the MoS_2 nanosheet will be dropped on the CdSe nanowire to form the 2D/1D heterostructure (Fig. S3d, Fig. S4f).

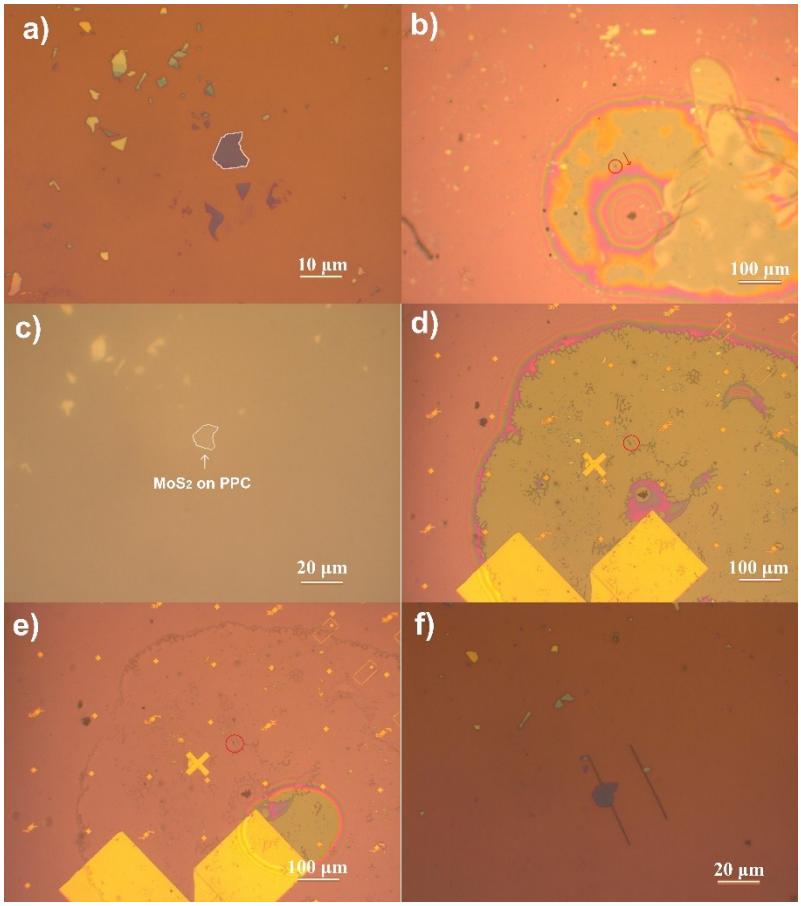

Figure S4. The optical images taken during the transfer. (a) Target MoS_2 nanosheet on a Si/SiO_2 substrate. (b) PPC contacted the MoS_2 nanosheet. (c) MoS_2 nanosheet on PPC picked up from the Si/SiO_2 substrate. (d) MoS2 nanosheet contacted the target CdSe nanowire. (e) PPC was lifted off slowly. (f) The fabricated MoS_2 nanosheet on CdSe nanowire heterostructure.

S4. Determination of MoS_2/CdSe band alignment

The determination of MoS_2/CdSe band alignment is based on the reported bandgaps, affinities and calculated work functions of MoS_2 nanosheet and CdSe nanowire. The reported bandgap values of MoS_2 (1.28 eV)[S1, S2] and CdSe (1.75 eV)[S3, S4], consistent with our photoluminescence measurement of the CdSe nanowire. The reported affinity values of MoS_2 and CdSe are 4.0 eV[S2, S5] and 4.7 eV[S6, S7], respectively. The work functions of MoS_2 and CdSe are 5.29 eV and 4.88 eV, respectively, based on the measured carrier concentrations and reported band structures by the following equations: $n = n_i e^{(E_F - E_i)/\kappa_B T}$, $p = n_i e^{(E_i - E_F)/\kappa_B T}$, $n_i^2 = N_c N_v e^{-\frac{E_c - E_v}{\kappa_B T}}$, where n and p are the carrier concentrations, n_i is the intrinsic carrier concentration; N_c and N_v are the equivalent density of states of conduction and valence bands, respectively; κ_B is the boltzmann's constant. N_c and N_v can be expressed as: $N_c = 2(\frac{2\pi m_n \kappa_B T}{h^2})^{3/2}$,$N_v = 2(\frac{2\pi m_p \kappa_B T}{h^2})^{3/2}$, respectively; where m_n and m_p are the effective masses of electron and hole, respectively. With that, the MoS_2/CdSe forms a type-II heterostructure with band offsets of conduction and valence bands of 0.70 eV and 1.20 eV, respectively.

S5. Light scattering at the 2D/1D heterostructure edges

In order to gain the structure details and describe the differences between these 2D/1D heterostructure edges, we have taken scanning electron microscope (SEM) images of these edges. As we can see, the nanowire between the right In/Au electrode and MoS_2 nanosheet was missing (Fig. S5d), which may be caused by the damage during the fabrication. During the measurements, the left In/Au electrode on CdSe nanowire was grounded, while the right In/Au electrode was suspended. In our laterally contacted structure, when a current flows across the heterojunction, the injected electrons and holes will meet at the 2D/1D heterostructure edge #1 first (Fig. S5e), due to the resistive nature of CdSe nanowire. Herein, as a direct band-gap semiconductor, which has a high electron-hole radiative recombination rate, the injected electrons and holes will mainly recombine in the CdSe nanowire and emit photons. Some of the emitted photons will scatter at the interface, while the rest will propagate in the CdSe nanowire, due to the waveguide nature of the CdSe nanowire. Due to the perfect 2D/1D interface at edge #1 (Fig. S5a), we can only observe a faint light spot at edge #1. The propagating light will be scattered when it meets the nanowire end facets or scattering points with abrupt geometry change[S8]. Therefore, we can explain the observed two strongest light spots at edge #2 and #4. At edge #2, we can see the MoS_2 nanosheet folds and ripples at the interface (Fig. S5b). This abrupt geometry change causes the light to be scattered. At edge #4, the nanowire end facet scatters light (Fig. S5d), due to its low reflectivity[S9]. Separately, at the edge #3, we observe a smooth contact between CdSe nanowire and MoS_2 nanosheet without an abrupt geometry change (Fig. S5c). Therefore, the light scattered at edge #3 may be too weak to be observed by the camera.

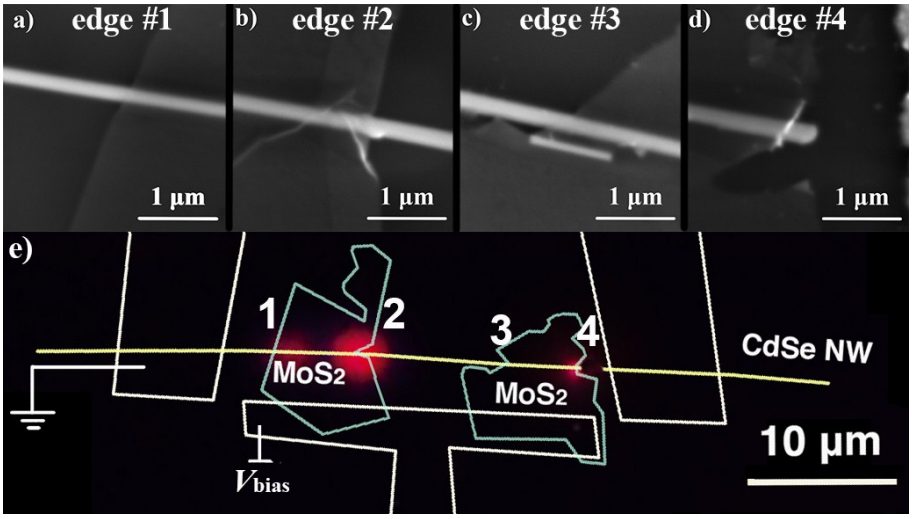

Figure S5. (a-d) SEM images of four 2D/1D heterostructure edges. (e) Electroluminescence (EL) optical image taken at a forward bias of 6 V. The 2D/1D heterostructure edges are numbered as 1 to 4 from left to right.

References:

S1. S. Han, H. Kwon, S. K. Kim, S. Ryu, W. S. Yun, D. Kim, J. Hwang, J.-S. Kang, J. Baik and H. Shin, Physical Review B, 2011, 84, 045409.

S2. H. Li, J. Wu, Z. Yin and H. Zhang, Accounts of chemical research, 2014, 47, 1067-1075.

S3. E. Kucur, J. Riegler, G. A. Urban and T. Nann, Journal of Chemical Physics, 2003, 119, 2333-2337.

S4. J. Jasieniak, J. Pacifico, R. Signorini, A. Chiasera, M. Ferrari, A. Martucci and P. Mulvaney, Advanced Functional Materials, 2010, 17, 1654-1662.

S5. S. Das, H. Y. Chen, A. V. Penumatcha and J. Appenzeller, Nano Letters, 2013, 13, 100.

S6. B. J. Landi, S. L. Castro, H. J. Ruf, C. M. Evans, S. G. Bailey and R. P. Raffaelle, Solar Energy Materials & Solar Cells, 2005, 87, 733-746.

S7. R. K. Swank, IEEE Transactions on Electron Devices, 1967, 153, 674-674.

S8. Y. Ye, L. Gan, L. Dai, H. Meng, F. Wei, Y. Dai, Z. Shi, B. Yu, X. Guo and G. Qin, Journal of Materials Chemistry, 2011, 21, 11760-11763.

S9. J. C. Johnson, H. Yan, R. D. Schaller, L. H. Haber, R. J. Saykally and P. Yang, The Journal of Physical Chemistry B, 2001, 105, 11387-11390.